REPORTS

GLASS STRUCTURE

Observation of the transition state for pressure-induced $BO_3 \rightarrow BO_4$ conversion in glass

Trenton Edwards,[1] Takatsugu Endo,[1] Jeffrey H. Walton,[2] Sabyasachi Sen[1]*

A fundamental mechanistic understanding of the pressure- and/or temperature-induced facile transformation of the coordination environment of boron is important for changing the physical properties of glass. We have used in situ high-pressure (up to 2 gigapascals) boron-11 solid-state nuclear magnetic resonance spectroscopy in combination with ab initio calculations to investigate the nature of the transition state for the pressure-induced $BO_3 \rightarrow BO_4$ conversion in a borosilicate glass at ambient temperature. The results indicate an anisotropic elastic deformation of the BO_3 planar triangle, under isotropic stress, into a trigonal pyramid that likely serves as a precursor for the subsequent formation of a BO_4 tetrahedron.

The importance of the local coordination environments of atoms in the lattice of crystalline matter and their response to pressure and temperature in understanding structure-property relations cannot be overstated (*1*). Coordination changes in glass-forming network liquids are responsible for generation of configurational entropy, controlling viscous flow and structural relaxation (*2*). Therefore, pressure- and/or temperature- (*P-T*) induced coordination changes have been studied fairly extensively in oxide glasses and liquids where the network-forming B, Al, and Si cations display increasing coordination numbers with increasing pressure and temperature (*2*–*12*). One of the most well-studied cases in this regard is the trigonal to tetrahedral $BO_3 \rightarrow BO_4$ conversion in borate and borosilicate glasses and liquids with increasing pressure and/or temperature (*5*–*12*). This B coordination change has pronounced effects on the structure-property relations in these materials relevant for their wide-ranging technological applications in fiber composites, radioactive waste encapsulation, and substrates for display (*9*, *11*). The $BO_3 \rightarrow BO_4$ conversion can be initiated in the supercooled liquid state just above the glass transition temperature T_g, and its magnitude can be strongly enhanced at relatively low pressures of a few hundred megapascals, often achieved in standard processing methods such as injection molding or hot press sintering (*9*).

Typically these structural changes are studied ex situ in glasses quenched from their parent liquids subjected to different *P-T* conditions. Thus, one loses the opportunity of monitoring the mechanism of coordination change in real time or of "seeing" the intermediate or transition state, although in certain favorable cases the transition state can be quenched (*4*). Furthermore, observation of time-dependent changes in the local coordination geometry requires application of an element-specific spectroscopic technique such as nuclear magnetic resonance (NMR) spectroscopy that is sensitive to subtle changes in short-range order. However, the application of solid-state NMR spectroscopy has remained limited largely to ambient pressure owing to the technological challenges associated with designing a high-pressure probe head with suitable nonmagnetic materials that can operate up to a few gigapascals and can allow for sufficient sensitivity and sample volume. Recently, we have designed a high-pressure NMR probe in our laboratory that can maintain hydrostatic pressures of up to 2.5 GPa (*13*). Here, we present the first results of an in situ high-pressure (up to 2.0 GPa) ^{11}B NMR spectroscopic study using this probe, in combination with ab initio calculations that directly demonstrate the nature of the transition state for $BO_3 \rightarrow BO_4$ conversion in a commercial borosilicate glass of Corning code 7059 (*13*) at ambient temperature.

The three NMR parameters that control the ^{11}B NMR line shapes in oxides include the isotropic chemical shift δ_{iso}, the quadrupolar coupling constant C_Q, and the electric field gradient asymmetry parameter η. These parameters are primarily controlled by the nearest-neighbor coordination

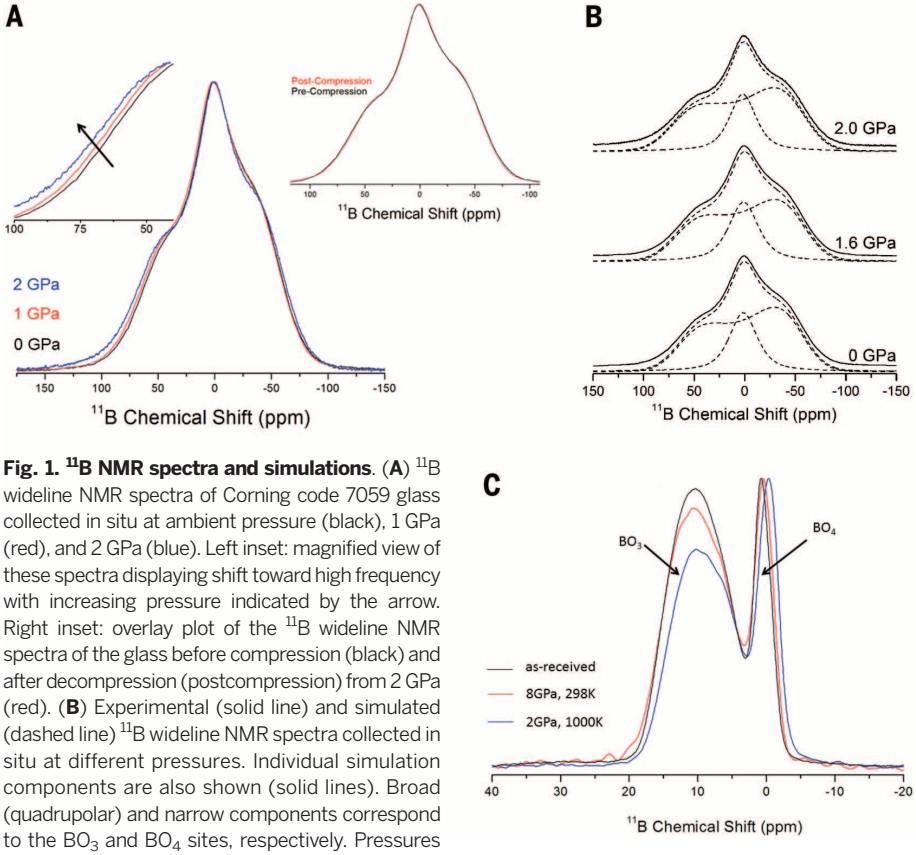

Fig. 1. ^{11}B NMR spectra and simulations. (**A**) ^{11}B wideline NMR spectra of Corning code 7059 glass collected in situ at ambient pressure (black), 1 GPa (red), and 2 GPa (blue). Left inset: magnified view of these spectra displaying shift toward high frequency with increasing pressure indicated by the arrow. Right inset: overlay plot of the ^{11}B wideline NMR spectra of the glass before compression (black) and after decompression (postcompression) from 2 GPa (red). (**B**) Experimental (solid line) and simulated (dashed line) ^{11}B wideline NMR spectra collected in situ at different pressures. Individual simulation components are also shown (solid lines). Broad (quadrupolar) and narrow components correspond to the BO_3 and BO_4 sites, respectively. Pressures are denoted alongside each spectrum. The simulated spectrum and the components are vertically offset with respect to the experimental spectrum for clarity. (**C**) ^{11}B MAS NMR spectra of the as-received glass (black) and of samples of the same glass quenched from 2 GPa and 1000 K (blue) and from 8 GPa and 298 K (red). Broad (quadrupolar) and narrow peaks correspond to the BO_3 and BO_4 sites, respectively, in the glass. All spectra are normalized to the BO_4 peak.

[1]Division of Materials Science and Engineering, University of California at Davis, Davis, CA 95616, USA. [2]Nuclear Magnetic Resonance Facility, University of California at Davis, Davis, CA 95616, USA.
*Corresponding author. E-mail: sbsen@ucdavis.edu

environment of the boron atom and, thus, vary over a relatively narrow range (*14*–*16*). The BO_3 trigonal planar environment with its approximate D_{3h} site symmetry is characterized by a ^{11}B NMR line shape that is controlled by quadrupolar interaction, whereas the BO_4 tetrahedral environment with the locally cubic T_d site symmetry of the central B atom results in a symmetric and relatively narrow Gaussian line shape. The experimental ^{11}B NMR line shape of the 7059 glass at various pressures (Fig. 1A) can be simulated well with two components corresponding to the BO_3 and BO_4 sites in the glass structure (Fig. 1B). The corresponding NMR simulation parameters for the two B sites are listed in table S1 (*13*). The BO_3:BO_4 ratio is ~75:25 at ambient conditions and is consistent with the value obtained from the simulation of the high-resolution ^{11}B magic angle spinning (MAS) NMR spectrum (76:24) of the as-received glass (Fig. 1C and table S2). This ratio at ambient temperature appears to remain unchanged with pressure, at least up to 2 GPa (table S1). This result is consistent with the observation that the BO_3:BO_4 ratio decreases only a small amount (74:26) upon quenching the glass from 8 GPa at ambient temperature, which is not surprising considering that coordination changes in oxide glasses at such low pressures require thermal activation (table S2). The role of thermal activation is evident when we compare the ^{11}B MAS NMR spectrum of the glass quenched from 2 GPa and 1000 K to that of the as-received glass and the glass quenched from 8 GPa at ambient temperature (Fig. 1C). The BO_3:BO_4 ratio of the sample quenched from 2 GPa and 1000 K is substantially lower (70:30) than that of both the as-received, ambient pressure glass (76:24) and the sample quenched from a higher pressure of 8 GPa at ambient temperature (74:26), indicating a pressure-induced $BO_3 \rightarrow BO_4$ conversion that is strongly facilitated by temperature (table S2).

The simulation of the in situ high-pressure ^{11}B NMR line shapes (Fig. 1, A and B) indicates that although the BO_3:BO_4 ratio and the quadrupolar parameters for the BO_3 site do not change significantly in this narrow pressure range (table S1), the ^{11}B isotropic chemical shift δ_{iso} for the BO_3 site shifts monotonically to higher frequency with increasing pressure at a nearly constant rate of ~1.6 parts per million (ppm)/GPa (Fig. 2). On the other hand, the ^{11}B δ_{iso} for the BO_4 sites does not display any significant change with pressure. In contrast, the ^{11}B δ_{iso} values for both BO_3 and BO_4 sites (15.9 and −0.3 ppm, respectively) show a clear shift toward low frequency (increasing shielding) in the case of the sample quenched from 2 GPa and 1000 K (table S2). The structural modification at high pressure corresponding to these changes in the ^{11}B NMR parameters cannot be understood a priori without a systematic understanding of the influence of any change in the BO_3 coordination geometry on the ^{11}B NMR parameters. To understand the evolution of the BO_3 units in the glass, we performed ab initio calculations of ^{11}B NMR parameters using density functional theory (DFT) on a molecule of H_3BO_3 containing a central B atom in triangular planar coordination with three OH groups (*13*). We consider the effects of three types of changes in the B coordination geometry on the ^{11}B NMR parameters.

The first model that we consider is a uniform compression or expansion of the B-O coordination triangle (model 1). This model results in a systematic change in the isotropic chemical shift δ_{iso} while the quadrupolar parameters C_Q and η remain constant (table S3). The ^{11}B δ_{iso} moves to lower frequencies upon shortening of the B-O bond lengths, at a rate of ~76.5 ppm/Å (Fig. 3A). The ^{11}B δ_{iso} of the BO_3 and BO_4 sites in the sample quenched from 2 GPa and 1000 K is shifted to a lower frequency compared to the ambient pressure sample. This shift may be indicative of a compression of the B-O bond length in the sample quenched from high *P-T*. Such a shift can also be attributed to an increased mixing of Si and B, resulting from the increasing concentration of BO_4 units combined with an avoidance in their connectivity via B-O-B linkages (*12*). By contrast, in situ high-pressure ^{11}B NMR experiments show a shift of the ^{11}B δ_{iso} of the BO_3 site to higher frequencies with increasing pressure, which would require a uniform expansion of the BO_3 triangle. Uniform expansion with increasing pressure is clearly unphysical, and thus this model cannot explain the experimental observation made by in situ high-pressure NMR.

The second model that we consider is an anisotropic, in-plane deformation (model 2), where one of the B-O distances is systematically increased while the other atom positions are allowed to relax within the B-O plane to a minimum-energy configuration. This mode of deformation results in a systematic and rapid increase in the quadrupolar asymmetry parameter η (table S4) that is inconsistent with the experimental observations made in this study. The ^{11}B NMR line shapes for the BO_3 site, obtained in situ or ex situ, indicate insignificant changes in η with pressure (tables S1 and S2).

The final model of deformation that we consider is to move the central B atom out of the plane of the oxygen atoms along the threefold symmetry axis while the B-O distances are allowed to relax (*13*). The out-of-plane displacement of the central B atom results in an increase in the B-O bond lengths and a change in the symmetry of the BO_3 environment from trigonal planar (D_{3h}) to trigonal pyramidal (C_{3v}). This mode of deformation affects the ^{11}B δ_{iso} appreciably (Fig. 3B), which moves monotonically to higher frequencies with increasing vertical out-of-plane displacement of the B atom. However, no significant changes in C_Q and η are observed (table S5). These results are consistent with the in situ high-pressure NMR spectra that demonstrate the high-frequency shift of ^{11}B δ_{iso} for the BO_3 site with increasing pressure, without any significant change in C_Q and η. Hence, the experimentally observed shift of 1.6 ppm/GPa for the BO_3 site in in situ high-pressure NMR indicates an average out-of-plane displacement of the B atom by ~0.26 Å/GPa, which would correspond to an increase in the average B-O distance of ~0.007 Å/GPa. This out-of-plane displacement of the central B atom in the BO_3 site is then fully reversible during compression-decompression cycle up to ~2 GPa (Fig. 1A).

Together, the NMR spectroscopy and DFT modeling results indicate that the elastic, out-of-plane

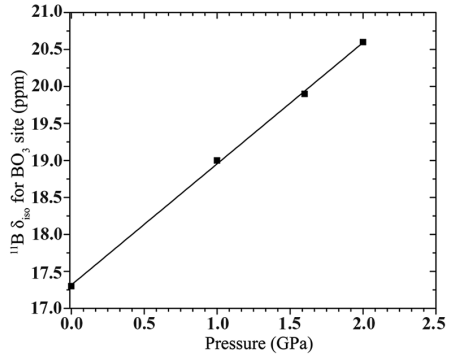

Fig. 2. Pressure change of ^{11}B NMR spectra. Variation of ^{11}B δ_{iso} for the BO_3 sites in Corning code 7059 glass with pressure as obtained from simulation of the ^{11}B wideline NMR spectra collected in situ at various pressures (see Fig. 1, A and B, and table S1). Solid line is a linear least-squares fit to the data points.

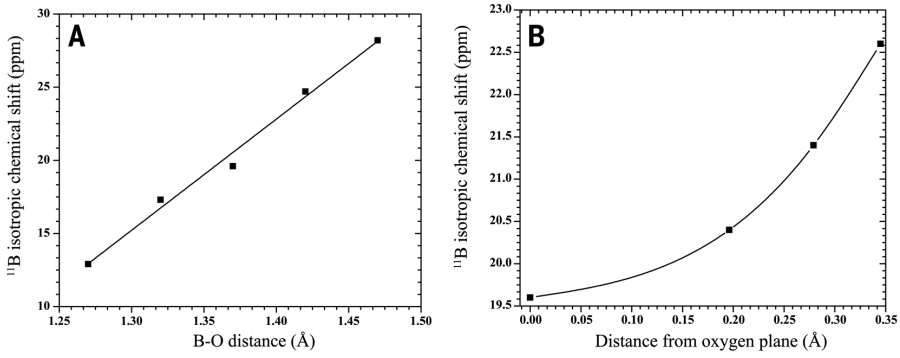

Fig. 3. Calculated change of model ^{11}B NMR parameters. (**A**) Variation of calculated ^{11}B δ_{iso} with B-O bond lengths in the H_3BO_3 molecule in model 1 (see text for details). Solid line is a linear least-squares fit to the data points. (**B**) Monotonic shift of calculated ^{11}B δ_{iso} to higher frequencies with increasing vertical out-of-plane displacement of the B atom in the H_3BO_3 molecule in model 3 (see text for details). Curved line through the data points is a guide to the eye only.

displacement of the central B atom in the BO_3 units best explains the pressure-induced changes observed in the in situ ^{11}B high-pressure NMR spectra. Although it may be counterintuitive at first to expect such anisotropic deformation of the BO_3 coordination environment under hydrostatic stress, an out-of-plane displacement of the B atom in the BO_3 unit is clearly a necessary step in its conversion into a BO_4 tetrahedron under pressure. The ultimate success of the $BO_3 \rightarrow BO_4$ coordination change must depend on the availability of a fourth oxygen atom in the structural neighborhood for bonding to the B atom, but the pressure-induced deformation of a BO_3 triangle into a trigonal pyramid clearly serves as a transition state for this conversion. Such pressure-induced displacement of the central B atom from the plane of the oxygen atoms is also expected to result in electric dipole moments in glass that can interact with light to strongly influence the photoelastic property (e.g., birefringence) of a borate glass (*17*). The application of in situ high-pressure solid-state NMR as a spectroscopic technique presents exciting opportunities in future in developing atomistic understanding of various stress-induced processes in amorphous materials.

REFERENCES AND NOTES

1. S. R. Elliott, *The Physics and Chemistry of Solids* (Wiley, New York, ed. 1, 1998).
2. G. N. Greaves, S. Sen, *Adv. Phys.* **56**, 1–166 (2007).
3. G. H. Wolf, P. F. McMillan, in *Structure, Dynamics and Properties of Silicate Melts*, J. F. Stebbins, P. F. McMillan, D. B. Dingwell, Eds., Reviews in Mineralogy, vol. 32 (Mineralogical Society of America, Washington, DC, 1995).
4. J. F. Stebbins, *Nature* **351**, 638–639 (1991).
5. S. Sen, Z. Xu, J. F. Stebbins, *J. Non-Cryst. Solids* **226**, 29–40 (1998).
6. S. Sen, *J. Non-Cryst. Solids* **253**, 84–94 (1999).
7. S. Sen, T. Topping, P. Yu, R. E. Youngman, Atomic-scale understanding of structural relaxation in simple and complex borosilicate glasses. *Phys. Rev. B* **75**, 094203 (2007).
8. S. S. Uzun, S. Sen, *J. Phys. Chem. B* **111**, 9758–9761 (2007).
9. L. Wondraczek, S. Sen, H. Behrens, R. E. Youngman, *Phys. Rev. B* **76**, 014202 (2007).
10. F. Angeli *et al*., *Phys. Rev. B* **85**, 054110 (2012).
11. F. Michel *et al*., *J. Non-Cryst. Solids* **379**, 169–176 (2013).
12. L.-S. Du, J. R. Allwardt, B. C. Schmidt, J. F. Stebbins, *J. Non-Cryst. Solids* **337**, 196–200 (2004).
13. Materials and methods are available as supplementary materials on *Science* Online.
14. G. L. Turner, K. A. Smith, R. J. Kirkpatrick, E. Oldfield, *J. Magn. Reson.* **67**, 544–550 (1986).
15. S. Kroeker, J. F. Stebbins, *Inorg. Chem.* **40**, 6239–6246 (2001).
16. S. Sen, *Mol. Simul.* **34**, 1115–1120 (2008).
17. M. Guignard, L. Albrecht, J. W. Zwanziger, *Chem. Mater.* **19**, 286–290 (2007).

ACKNOWLEDGMENTS

T. Edwards and S.S. were supported by a grant from the National Science Foundation (NSF-DMR 1104869). T. Endo was supported by a postdoctoral fellowship for research abroad by the Japan Society for Promotion of Science.

SUPPLEMENTARY MATERIALS

www.sciencemag.org/content/345/6200/1027/suppl/DC1
Materials and Methods
Figs. S1 to S5
Tables S1 to S5
References (*18*–*28*)

19 May 2014; accepted 15 July 2014
10.1126/science.1256224

STELLAR DISTANCES

A VLBI resolution of the Pleiades distance controversy

Carl Melis,[1]* Mark J. Reid,[2] Amy J. Mioduszewski,[3] John R. Stauffer,[4] Geoffrey C. Bower[5]

Because of its proximity and its youth, the Pleiades open cluster of stars has been extensively studied and serves as a cornerstone for our understanding of the physical properties of young stars. This role is called into question by the "Pleiades distance controversy," wherein the cluster distance of 120.2 ± 1.5 parsecs (pc) as measured by the optical space astrometry mission *Hipparcos* is significantly different from the distance of 133.5 ± 1.2 pc derived with other techniques. We present an absolute trigonometric parallax distance measurement to the Pleiades cluster that uses very long baseline radio interferometry (VLBI). This distance of 136.2 ± 1.2 pc is the most accurate and precise yet presented for the cluster and is incompatible with the *Hipparcos* distance determination. Our results cement existing astrophysical models for Pleiades-age stars.

Robust physical parameters for stars can only be obtained when an estimate of the distance to the object of interest exists. Trigonometric parallax, which uses the orbit of Earth around the Sun to inform the principle of triangulation, provides the most fundamental distance measurement outside of our solar system. High-precision tests of stellar physical models thus rely heavily on collections of parallax determinations. With reasonable physical models for nearby stars—and some mild assumptions about the homogeneity of classes of astrophysical objects throughout the universe [the Vogt-Russell theorem; see, e.g., (*1*, *2*)]—distance estimates for sources that lie beyond the current limit of trigonometric parallax can be systematically compiled. Such a methodology forms the basis of the cosmic distance ladder that elucidates the structure and evolution of the universe (*3*).

Clusters of coeval stars yield a solid foundation for tests of stellar physical models. Young open clusters are especially important because their stellar constituents define the "zero-age main sequence," the curve along which stable, core-hydrogen–burning stars reside in a color-magnitude diagram. Empirical isochrones developed from these young open clusters can be applied to other vastly more distant groups of stars (when brightness measurements of individual stars in the group can be made) to estimate their distance, thus providing structural information for the galaxies that contain them (*4*, *5*). The Pleiades open cluster of stars is critical for such studies because its relatively young age places many of its stars on the zero-age main sequence. It is the closest cluster to Earth of its age and richness of stars and thus lends itself to highly detailed investigations. One would expect that all astrophysical parameters for such an important sample of stars would be well characterized. However, there still rages an open debate regarding the distance to the Pleiades.

Figure 1 summarizes distances obtained for the Pleiades cluster to date, including the new measurement described here. As can be seen, most measurements are in rough agreement with that produced in this work, with the stark exception of the *Hipparcos* astrometric satellite distances. For a single object near the distance of the Pleiades, *Hipparcos* was not capable of producing a distance measurement with accuracy better than 10%. However, by taking the aggregate of many cluster members, *Hipparcos* was able to achieve a Pleiades parallax with roughly 1% precision (*6*, *7*). In almost any other case, one would simply discard the disagreeable *Hipparcos* cluster distances as bad measurements, but the *Hipparcos* mission represents the most complete astrometric survey of the sky and of the Pleiades cluster to date. It provides a path that is free of stellar physical models to obtaining the cluster distance and combines more than 50 cluster-member distance measurements. Other methods either include at most several cluster members in their distance determination, rely heavily on physical models to obtain a cluster distance (whereas it should be the distance measurement that informs the development of physical models), or result in large uncertainties in the cluster distance.

Although the discrepancy between *Hipparcos* and the average non-*Hipparcos* distance (Fig. 1) amounts to a 10% difference, the resultant changes to physical models needed to obtain agreement with the *Hipparcos* value are quite significant.

[1]University of California, San Diego, Center for Astrophysics and Space Sciences, 9500 Gilman Drive, La Jolla, CA 92093-0424, USA. [2]Harvard-Smithsonian Center for Astrophysics, 60 Garden Street, Cambridge, MA 02138, USA. [3]National Radio Astronomy Observatory, Array Operations Center, 1003 Lopezville Road, Socorro, NM 87801, USA. [4]Spitzer Science Center (SSC), 1200 East California Boulevard, California Institute of Technology, Pasadena, CA 91125, USA. [5]Academia Sinica Institute of Astronomy and Astrophysics (ASIAA), 645 North A'ohoku Place, Hilo, HI 96720, USA.
***Corresponding author. E-mail: cmelis@ucsd.edu**

Observation of the transition state for pressure-induced $BO_3 \rightarrow BO_4$ conversion in glass

Trenton Edwards *et al.*

Science **345**, 1027 (2014);
DOI: 10.1126/science.1256224

Science (print ISSN 0036-8075; online ISSN 1095-9203) is published weekly, except the last week in December, by the American Association for the Advancement of Science, 1200 New York Avenue NW, Washington, DC 20005.